To be published, *Journal of Directed Energy*

Calibration and Testing of Distributed Fiber Optic Sensors for Detection of High Energy Radiation

Mathew Kautzman* and Brian Jenkins

Electrical and Computer Engineering Department, United States Naval Academy, Annapolis, Maryland 21402

Peter Joyce and Cody Brownell

Mechanical Engineering Department, United States Naval Academy, Annapolis, Maryland 21402

Development of technologies to detect high-energy laser (HEL) strikes on aircraft is of increasing interest due to recent advances in HEL weapons. These aircraft are manufactured using composite materials such as carbon fiber–reinforced polymer (CFRP). By embedding sensors into CFRP to detect HEL strikes, counter-directed energy weapons (CDEW) technology can be incorporated during the aircraft manufacturing process. Various kinds of sensors can be embedded in such composites during production of the vehicle. This research specifically focuses on the use of embedded, distributed optical-fiber sensors (DOFS) based on Raleigh scattering. Strain and temperature data are acquired from the sensor using the Luna Innovations' Optical Distributed Sensor Interrogator (ODiSI-B), primarily to measure temperature at the instant of a HEL strike. The interrogator can acquire data at 100-Hz and 23.8-Hz scan modes with strain and temperature precision of 1 με and 1 °C, respectively. The sensors used in this project are 1 m in length and measure strain and temperature with a spatial resolution of approximately 1 mm. A CFRP was designed and fabricated with a distributed optical fiber strain sensor woven between the plies of the carbon fiber fabric. To determine the temperature response of a DOFS up to 900 °C, a calibration technique was developed using K-type thermocouples. The DOFS was heated to high temperatures in a tube furnace while the sensor was interrogated. Once the DOFS temperature response was calibrated, the fabricated CFRP test article was assaulted with a HEL and the temperature response was measured.

KEYWORDS: HEL, CFRP, Detection, Calibration, Distributed optical fiber sensors

Received April 3, 2018; revised July 24, 2018.
*Corresponding author; email: mskautzman@gmail.com.

Nomenclature

HEL	high energy laser
CFRP	carbon fiber–reinforced polymer
DEW	directed energy weapon
CDEW	counter-directed energy weapon
T	temperature
f	frequency
A_i	coefficient of temperature-sensitivity function

1. Introduction

Directed energy weapon (DEW) production has increased over the last decade in the United States, China, and Russia, as well as other countries. DEWs have tested to be extremely efficient and accurate when shooting aircraft down during test trials for the US military. DEWs continue to be funded for production and implementation into the military.[1] Both the United States and foreign adversaries continue to fund and research DEWs and, as a result, counter-directed energy weapons (CDEWs) are needed to detect and respond to an energy strike before major damage occurs inside the delivery aircraft. Researchers and military-invested institutions are interested in developing materials for application in aircraft and other military vehicles that both protect and detect localized, high-temperature gradients within microseconds. Various methods have been studied and applied to produce composite materials with the capability to detect HEL strikes. Some examples of current methods used to monitor the structural health of composite materials consist of strain gauges, accelerometers, ultrasonic sensors, and passive acoustic sensors.[2] Optical fiber temperature sensors such as fiber Bragg gratings (FBGs) and distributed fiber optic sensors have also been studied recently.[3] Integrating these temperature sensors within composite structures could revolutionize materials used in military-grade vehicles. Fiber-optic sensor data can be rapidly acquired in real time. However, the detection speed of strain and temperature variations when using an embedded sensor is limited by the thermal response time of the composite. Therefore, the goal of this project is to develop a specific distribution of fiber optic sensors that maximizes the speed of response to directed, high-powered energy while also localizing the area targeted.

If distributed optical-fiber sensors (DOFS) can detect the strike before significant damage occurs, further impairment to the structure may be avoidable. Prior to testing the embedded fiber sensors using a high-energy laser (HEL) strike, the sensors need to be calibrated at high temperatures and embedded within the polymer matrix composite. The calibration ensures that the temperature of the composite is correctly measured by the sensor during the laser strike. In addition, the correct method of fabrication and location of the distributed optical fibers sensors within the carbon fiber–reinforced polymer (CFRP) is critical to avoid damage to the sensors and to measure the temperature response of the HEL. Successfully embedding the calibrated sensors is vital to perform research in HEL detection using distributed fiber sensors in embedded CFRPs.

Past research has shown that embedded FBGs can be used to accurately measure the temperature and location of HEL strikes on composites.[3] However, as point sensors,

numerous FBGs must be dispersed throughout the composite to accurately identify the location of a strike. In contrast, DOFS are longer sensors with much finer resolution along the entire length of the fiber. DOFS can locate the HEL strike more precisely, and provide greater accuracy in determining the speed of response for the sensor.

This research presents a high-temperature calibration technique for DOFS that limits sensor damage. The method used to embed a calibrated DOFS into CFRP composites is discussed. The CFRP composites are then tested to analyze response speed and location of HEL strikes. A synchronization technique is used that ensures precise measurements of the HEL detection speed using embedded sensors.

2. Background

Distributed sensors based on Rayleigh backscattering are produced using optical fiber made of silica with small variations in fiber density. Each fiber sensor has an individual "fingerprint" or signature that is uniquely dependent on the random index of refraction along the length of the optical fiber. Optical frequency–domain reflectometry is used to detect changes in temperature and strain. This is an interferometric method whereby light from a laser is split to produce a reference beam and a measurement beam. The measurement beam is then reflected from the sensor and recombined with the reference beam using a coupler as seen in Fig. 1.

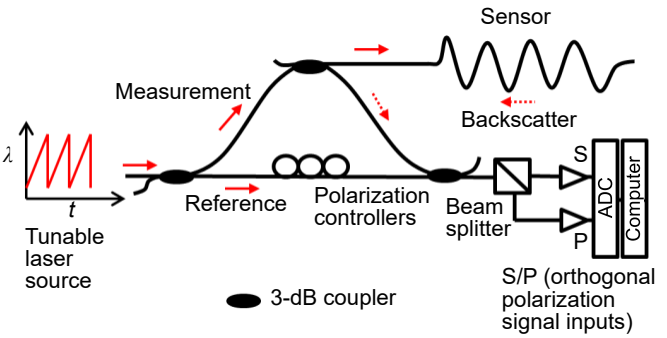

Fig. 1. Schematic demonstrating optical frequency–domain reflectometry.[4]

Changes in temperature and strain temporarily alter the back-reflected signal from the optical fiber sensor. After separating the combined beams into orthogonal polarizations, the Fourier transform of these signals provides amplitude and phase information that can be used to determine changes in strain or temperature.[4] A DOFS interrogator reads the backscatter amplitudes gathered during the tests and performs the Fourier transform of the signals. When compared to the reference state of the sensor, cross correlation yields a frequency shift that corresponds to any change in strain or temperature, determined using calibration coefficients to relate temperature or strain to frequency. Fig. 2 demonstrates how a frequency shift is calculated using the backscatter measurement.

Research by Rahim et al. used a method to calibrate DOFS to higher temperatures in a 5-month test at a constant temperature of 550 °C.[4] The test used thermocouples to measure the temperature in a small box furnace. The thermocouple readings were used to calibrate the sensitivity using a fourth-order polynomial,

$$T = 45.496 - 0.778(f) - 6.165E^{-4}\,(f^2) - 8.052E^{-7}(f^3) - 4.55E^{-10}(f^4) \quad (1)$$

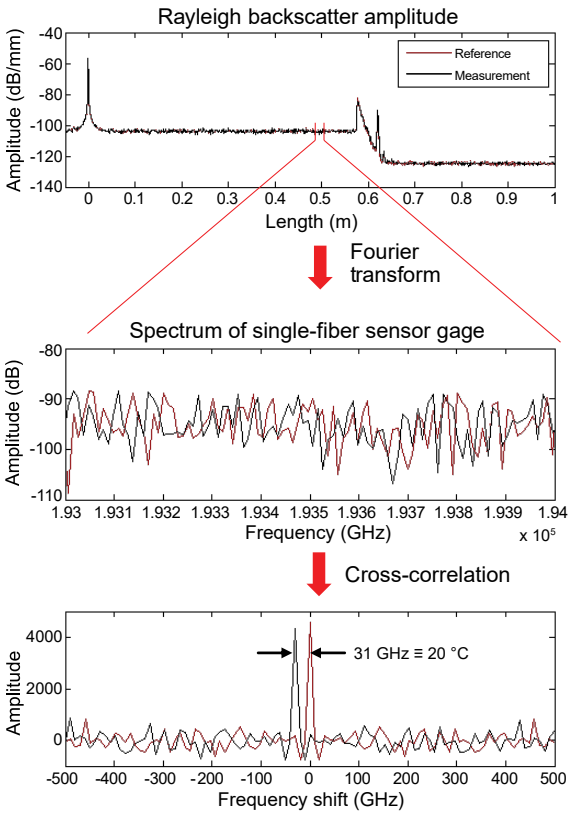

Fig. 2. Frequency shift calculation from Rayleigh scatter measurement.[4]

where the temperature T depends on frequency shift f. The temperature with respect to time and location in the fiber on day 56 of their test is shown in Fig. 3.

While these tests measured the sensor response at a steady temperature of 550 °C, it was unknown how the temperature sensors would react under faster changes in temperature, as would occur during a HEL strike at temperatures higher than 550 °C. IR camera and FBG measurements have indicated that temperatures within composites are higher than 1000 °C during HEL strikes.[5] The distributed sensors used in the experiments presented here—single-mode, low-bend loss fibers (SMF-LBL) with polyimide coating—had not been calibrated or ever exposed to temperatures this high. To prevent damage during

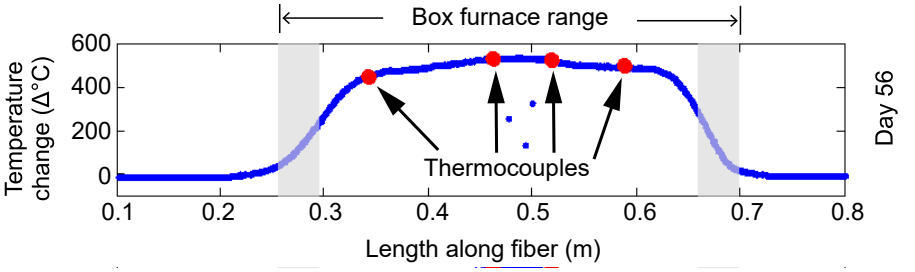

Fig. 3. Thermocouple and fiber temperature analysis by fiber position.[4]

calibration, a technique was developed that ensured the sensors would not be exposed to excessively high temperatures for too long during calibration, and temperatures were limited to 900 °C.

3. Method for DOFS Embedding into 5-Ply CFRP Composite

Five plies of carbon fabric were cut in 30-cm by 3-cm rectangles and laid on a smooth granite surface. To practice embedding the DOFS into the carbon fiber fabric, an optical fiber was woven into individual tows of the fabric, as seen in Fig. 4.

Specifically, the optical fiber was woven into the fabric four times: one at each end of the fabric and at two evenly spaced locations across the fabric. The fiber was embedded in a similar manner in the third and fifth plies of the composite. Once the fiber was woven into the fabric, resin was applied to the first ply. The second layer of carbon fabric (without an embedded DOFS) was then placed on top of the bottom layer to provide spacing between the plies with the sensor. More resin was applied to the second layer during the addition of each ply. The third layer (second ply with DOFS) was then placed on top of the second layer with the optical fibers aligned at each end, as seen in Fig. 5.

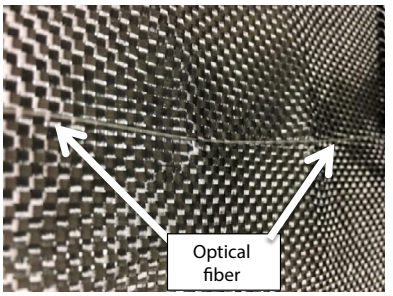

Fig. 4. Woven optical fiber into single ply of carbon fabric.

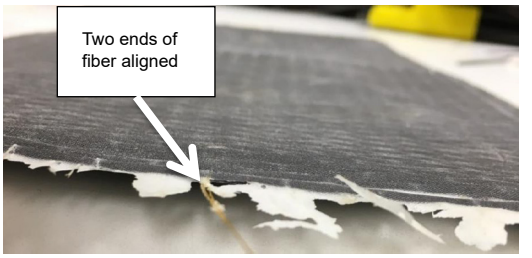

Fig. 5. 2-Ply carbon fiber–reinforced polymer with two ends of distributed sensor directly above one another.

When embedding the sensor into the CFRP, an optical fiber loop was formed outside the composite on each end. To ensure that the fiber does not break on either end, the loops must be larger than the minimum radius of the fiber curvature. The DOFS was aligned vertically in the first, third, and fifth plies. A schematic of the finished DOFS embedded CFRP is shown in Fig. 6.

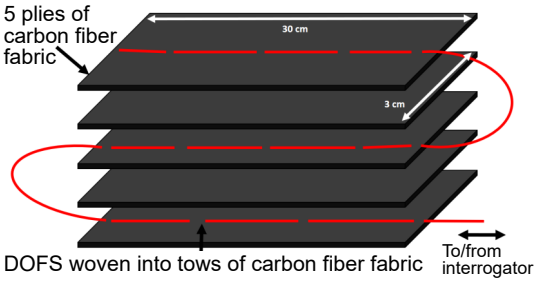

Fig. 6. Schematic showing looping of sensor due to layering of fabric plies.

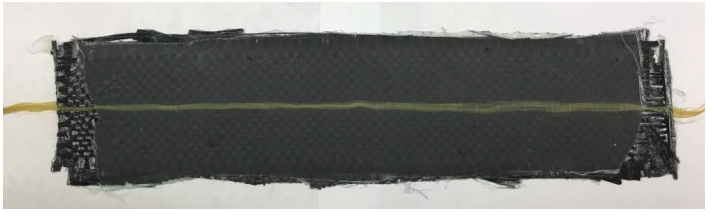

Fig. 7. Final 5-ply CFRP composite with embedded DOFS.

Lastly, after the resin dried, the CFRP was carefully removed from the granite surface to prevent damage to the sensor. A sharp tool was used to pry the specimen from the table without much bending of the composite. The final CFRP composite with an embedded DOFS is seen in Fig. 7 with yellow Kevlar yarn marking the position of the DOFS along the length of the specimen.

4. Preliminary Experiments for Calibration

To properly calibrate a DOFS, preliminary tests were completed to determine the best high-temperature calibration technique. Initially, a 30-cm–long tube furnace with a 2.5-cm inner diameter was aligned vertically to allow for easier insertion of the optical fiber. However, (vertical) heat convection prevented stable furnace temperatures, so a horizontal furnace orientation was chosen as the best option for calibration. The tube furnace used to calibrate the DOFS can reach temperatures as high as 1100 °C, in increments of 1 °C.

Preliminary testing of the furnace used five evenly spaced thermocouples attached to a steel rod to measure the temperature gradient inside the furnace during the heating cycle. However, the steel rod warped during the initial tests, so quartz tubes were used instead during actual calibration tests. The thermocouples for the initial horizontal test were located at marks 5.08 cm, 10.16 cm, 15.24 cm, 20.32 cm, and 25.40 cm along the length of the furnace. The testing structure appears in Fig. 8.

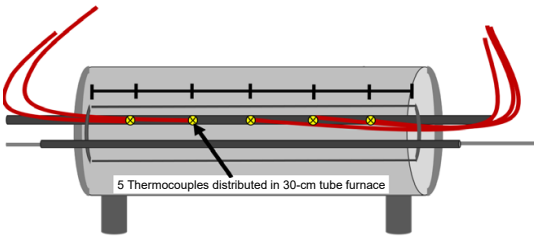

Fig. 8. Horizontal tube furnace orientation showing approximate thermocouple locations.

To test the furnace heating cycle, the furnace was set at 100 °C and incremented by 100 °C until reaching 900 °C. At every increment, 2 minutes were allowed for the thermocouples to stabilize at that temperature. Fig. 9 shows the data for the horizontal furnace test.

While the heating cycle in Fig. 9 for the horizontal test was better behaved than for the vertical test, the test indicated that the tube furnace temperature was not symmetric around the center, as had been anticipated. Further testing demonstrated that sufficient time (approximately 15 min) was needed for the temperature to stabilize within the furnace, at which point temperatures were symmetrically distributed around the tube furnace center.

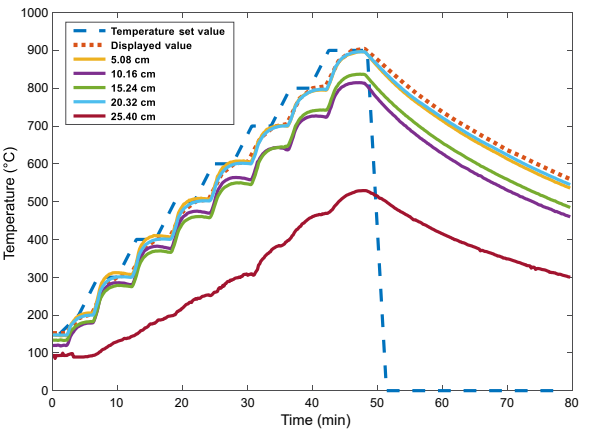

Fig. 9. Initial horizontal tube furnace temperature measurements.

5. DOFS Calibration Method

The distributed fiber optic sensors used in these tests can withstand temperatures near 350 °C before the outer coating begins to melt and char. Additionally, prolonged exposure to temperatures over 700 °C begins to degrade performance of the sensor itself. Hence, to prevent damage to the sensor during calibration at high temperatures, quartz rods were used to rapidly insert and retract the sensor from the tube furnace. Quartz rods were used instead of steel rods to avoid warping at high temperatures. Before calibration, a DOFS was attached to the outside of a 6-mm, outer-diameter (OD) quartz tube using Kapton tape. The 6-mm tube was oriented to slide along a second quartz tube with a 2-mm OD. The diagram in Fig. 10 provides a visual representation of the method used to rapidly insert and remove the DOFS.

The temperature of the tube furnace was set to its desired value and held long enough for the thermocouple readings to stabilize. Once the temperature had stabilized, the DOFS was quickly inserted into the furnace. The data logger for the thermocouples and the Luna interrogator system simultaneously recorded data for 2–3 s. Immediately after data were collected, the DOFS was removed from the tube furnace, the temperature of the tube furnace was incremented, and the process was repeated until all measurements were complete.

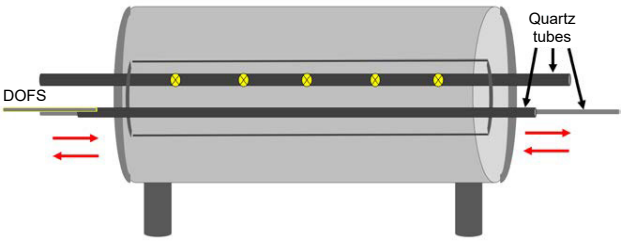

Fig. 10. Calibration schematic of DOFS attached to quartz tubes inside tube furnace.

300-°C DOFS calibration

The frequency shift measurements generated by the Luna interrogator are gathered from the cross-correlation of the measured beam and reference beam, as shown in Fig. 1. Those shifts can be converted into temperature changes (ΔT) by using a temperature-sensitivity function such as the following:

$$\Delta T = A_0 + A_1(f) + A_2(f^2) + A_3(f^3) + A_4(f^4) \quad (2)$$

ΔT is dependent on the frequency shift (f), based on coefficients that can be modified after calibration. The default temperature sensitivity used by the Luna interrogator is given by:

$$\Delta T = -0.6380\ (f) \quad (3)$$

where f is given in gigahertz and temperature change in degrees Centigrade. Eq. 3 applies at lower temperatures, at which the response is linear with respect to frequency. However, linear sensitivity is only accurate up to about 250 °C.[4] For experimental temperatures that surpass 250 °C, the DOFS interrogator must be calibrated to accurately measure higher temperatures.

A 300-°C DOFS calibration was performed to ensure that the technique for rapidly gathering interrogator and thermocouple data would be sufficient. The test was also used to refine the MATLAB code used to calculate the coefficients in Eq. 2. The coefficients were determined using a least-squares fit, by comparing the temperature data measured by the DOFS within the furnace to the actual temperature measured by the thermocouples. The furnace temperature ranged from 50 °C to 300 °C in 50-°C increments. At each temperature, the fiber was inserted into the tube furnace, data were collected, and the sensor was removed. Seven total trials at the different tube furnace temperature settings were performed, including an initial trial at ambient temperature. Resulting coefficients associated with each thermocouple position are shown in Table 1 for a fourth-order polynomial fit. To determine the sensitivity function that applies to the entire sensor length based on Eq. 2, the coefficients for the five thermocouple positions were averaged.[4] The resulting sensitivity function for the 300-°C calibration is shown in Eq. 4.

$$\Delta T = 0.6024 - 0.6605\,(f) - 5.6080E^{-4}\,(f^2) - 3.8290E^{-6}(f^3) - 5.6936E^{-9}(f^4) \quad (4)$$

Table 1. 300-°C Temperature Sensitivity–Function Coefficients Using Quartic Fit by Location

Location (m)	Constant (°C)	Linear (°C/GHz)	Quadratic (10^{-4} °C/GHz^2)	Cubic (10^{-6} °C/GHz^3)	Quartic (10^{-9} °C/GHz^4)	R^2
0.0400	–0.3387	–0.6083	7.3348	4.1955	6.1418	0.9997
0.0998	–3.5272	–0.7804	9.7125	2.0462	3.7064	0.9999
0.1491	0.8411	–0.7013	4.0428	3.3888	4.9979	1.0000
0.1990	2.2162	–0.6210	8.9568	4.3305	5.4715	0.9999
0.2489	3.8207	–0.5911	8.6765	5.1836	8.1499	0.9998
Average	0.6024	–0.6605	5.6080	3.8290	5.6936	0.9999

900-°C DOFS calibration

After demonstrating that the calibration technique worked properly at 300 °C, the DOFS was calibrated to 900 °C. The tube furnace temperature was varied from 75 °C to 900 °C in 75-°C increments. Hence, the DOFS was calibrated at 13 temperatures from room temperature to 900 °C. MATLAB was used determine linear, cubic, and quartic polynomials to fit the Luna interrogator data to the actual thermocouple measurements. Fig. 11 shows the error that results when using the default temperature sensitivity function in Eq. 3.

Circles in Fig. 11 are the thermocouple measurements at each tube furnace setting. Colored curves are the interrogator temperatures at each tube furnace setting using the linear fit in Eq. 3. The linear fit is accurate only to 250 °C, and quickly becomes unreliable at higher temperatures. To determine a better fit for the data in Fig. 11, coefficients were generated for both third- and fourth-order polynomials using MATLAB. Resulting coefficients are shown in Tables 2 and 3. For comparison, coefficients for the quartic fit to 550 °C in Rahim et al.[4] are also shown in Table 4. There is general agreement between this research and Rahim et al.[4]; the only significant difference between Tables 3 and 4 is for the constant

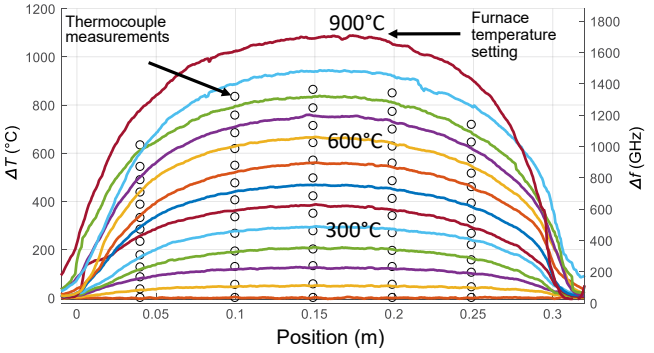

Fig. 11. Temperature and frequency measurements at various temperatures using default linear fit across position of tube furnace.

coefficient A_0, defined in Eq. 2. For the calibration results in Tables 2 and 3, A_0 is expected to be closer to 0 °C since Eq. 2 in this research predicts the temperature shift away from room temperature, rather than actual temperature.

As before, the coefficients at each position were then averaged to generate a polynomial fit of sensor temperatures to thermocouple temperatures that applies across the full length of the sensor. Based on Table 2, the cubic temperature sensitivity is given by:

$$\Delta T = 5.3656 - 0.6284(f) - 1.0262E^{-4}\,(f^2) - 1.9677E^{-8}(f^3) \qquad (5)$$

Table 2. Temperature Sensitivity Coefficients for Cubic Fit by Location

Location (m)	Constant (°C)	Linear (°C/GHz)	Quadratic (10^{-4} °C/GHz^2)	Cubic (10^{-8} °C/GHz^3)	R^2
0.0400	2.3533	–0.6900	–2.2630	–6.9305	0.9947
0.0998	5.2699	–0.6385	–0.9028	–1.0622	0.9995
0.1491	6.5815	–0.6069	–0.5472	–0.1201	0.9995
0.1990	6.9441	–0.6078	–0.4607	–0.6051	0.9996
0.2489	5.6791	–0.5989	–0.9570	–2.5710	0.9992
Average	5.3656	–0.6284	–1.0262	–1.9677	0.9985

Table 3. Temperature Sensitivity Coefficients for Quartic Fit by Location

Location (m)	Constant (°C)	Linear (°C/GHz)	Quadratic (10^{-4} °C/GHz^2)	Cubic (10^{-7} °C/GHz^3)	Quartic (10^{-10} °C/GHz^4)	R^2
0.0400	1.9122	–0.7013	–2.7265	–1.3051	–0.2513	0.9947
0.0998	–1.6615	–0.7662	–4.7988	–3.9677	–1.2000	0.9998
0.1491	–0.1204	–0.7287	–4.1076	–3.3498	–0.9937	0.9998
0.1990	1.2748	–0.7169	–3.7704	–3.1699	–0.9850	0.9999
0.2489	0.1582	–0.7249	–5.5370	–5.5911	–1.9351	0.9995
Average	0.3127	–0.7276	–4.1881	–3.4767	–1.0730	0.9987

Using Table 3, the quartic temperature sensitivity is expressed as:

$$\Delta T = 0.3127 - 0.7276(f) - 4.1881E^{-4}\,(f^2) - 3.4767E^{-7}(f^3) - 1.0730E^{-10}(f^4) \quad (6)$$

Resulting plots of the linear, cubic, and quartic polynomials using Eqs. 3, 5, and 6 are shown in Fig. 12. The largest thermocouple temperature measured during the 900 °C calibration was 887 °C, corresponding to an approximate shift of 860 °C from room temperature. The linear fit, based on specified performance from the sensor vendor is only valid to 250 °C. In contrast, both the cubic and quartic calibrations performed here are valid to 860 °C. However, Fig. 12 shows that the quartic fit is not useful for extrapolations to temperatures above 860 °C because of the natural shape of a quartic function. The cubic fit is more accurate for extrapolation to temperatures greater than 860 °C, which are expected to occur during an HEL strike.

Table 4. Luna Quartic Fit Calibration Coefficients[4]

Location (m)	Constant (°C)	Linear (°C/GHz)	Quadratic (10^{-4} °C/GHz^2)	Cubic (10^{-7} °C/GHz^3)	Quartic (10^{-10} °C/GHz^4)	R^2
0.025	45.797	–0.777	–6.385	–8.908	–5.360	0.9999
0.153	45.477	–0.781	–6.226	–8.014	–4.455	0.9999
0.306	45.975	–0.775	–5.885	–7.233	–3.850	0.9999
Average	45.496	–0.778	–6.165	–8.052	–4.555	0.9999

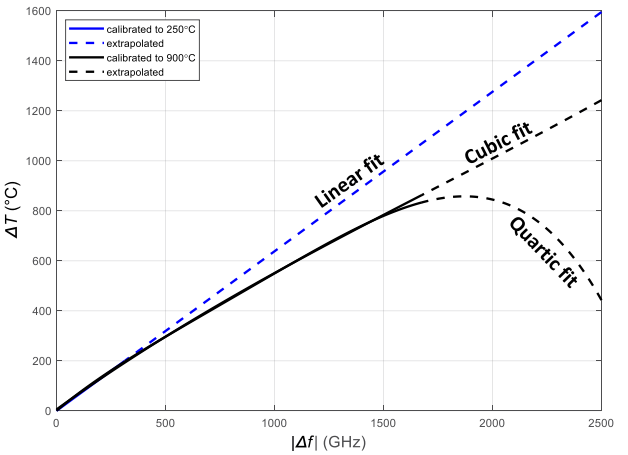

Fig. 12. DOFS sensitivity based on linear, cubic, and quartic polynomial fit coefficients.

To determine the cubic fit accuracy, Fig. 13 shows the temperature change at various tube furnace positions after Eq. 5 is applied to the frequency data gathered from the interrogator. In comparison to Fig. 11, it is evident from Fig. 13 that the sensitivity as expressed by the Eq. 5 gives much better agreement with the thermocouple measurements than a linear fit. Fig. 14 shows a plot of the normalized residuals, that is, the difference between the circles (thermocouple temperatures) in Fig. 13 and the sensor temperatures based on Eq. 5, normalized to the thermocouple temperature. The cubic fit results in a maximum normalized residual of 9% when calibrating up to 875 °C. In comparison, the residuals for the quartic sensitivity function in Eq. 6 to 875 °C were nearly identical to those shown

in Fig. 14, so there is no loss of accurate results at temperatures below 875 °C by using a third-order polynomial instead of a fourth-order polynomial.

The 900-°C calibration test developed coefficients for the temperature sensitivity function of the DOFS interrogator to accurately measure temperatures up to about 860 °C. Temperature measurements higher than 860 °C can be extrapolated using the cubic fit.

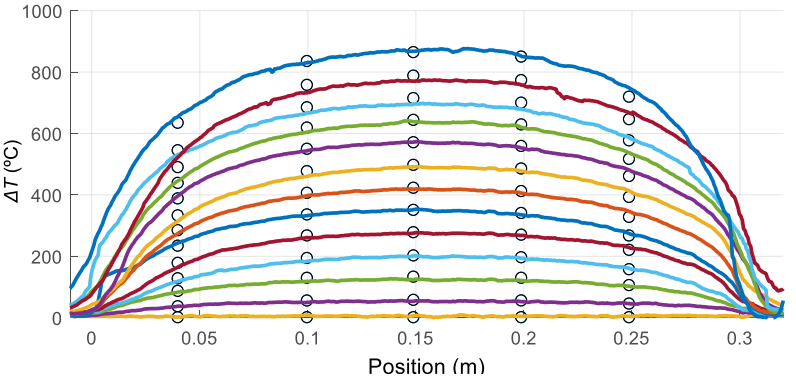

Fig. 13. Processed frequency data with cubic fit in comparison to thermocouple measurements (as shown at circles).

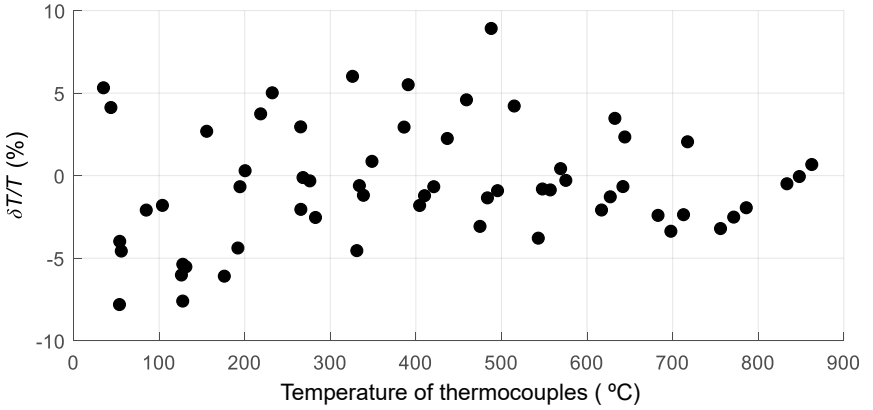

Fig. 14. Cubic fit residuals normalized to thermocouple temperatures.

6. HEL Strike Setup and Procedure

The schematic used for all HEL strikes is shown in Fig. 15. A 1064-nm laser with mean irradiance of approximately 250 W/cm^2 was directed toward a 90/10 beam splitter. At the HEL wavelength, the beam split into two paths, with 93% of the power (232.1 W/cm^2) in a strike beam and 7% of the power (17.5 W/cm^2) in a sync (synchronization) beam. The strike beam was reflected toward a mirror and directed toward the composite. The sync beam served as a precise reference to indicate when the laser turned on to measure speed of response; hence, the sync beam was always aimed directly onto the sensor. The strike

beam varied its position on the specimen from strike to strike, either by adjusting the mirror or the composite.

Seven HEL strikes were conducted during the HEL tests. The detection time of each strike was compared to the turn-on time of the sync beam, which was incident on the composite at the same position for every test. The strike locations (shown in Fig. 16) vary from 2 cm, 1 cm, or 0.5 cm above or below the sensor. As is apparent in Fig. 16, a strike left char on the specimen indicating the presence of flames that were directed upward during each strike.

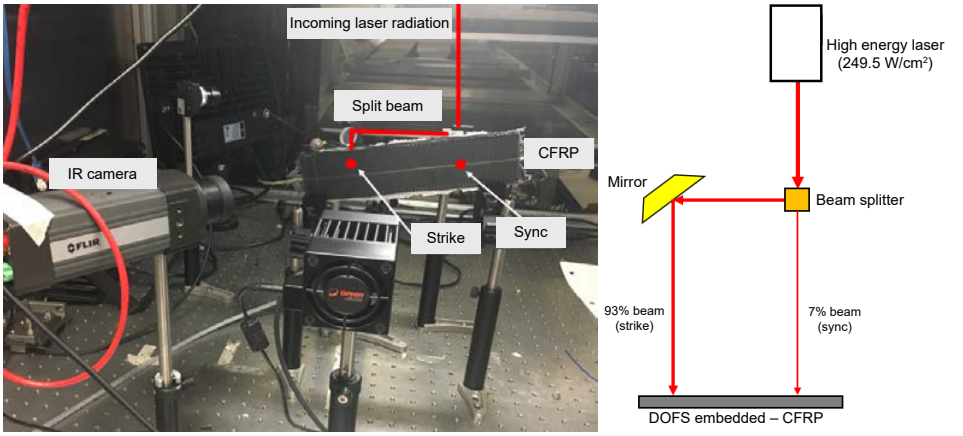

Fig. 15. HEL strike schematic and diagram.

The final strike was a direct strike with 93% irradiance concentrated directly on the DOFS embedded into the carbon fiber–reinforced polymer composite. This strike destroyed the sensor. After the strikes were conducted, the data were post-processed using the calibrated third-order polynomial in Eq. 5 to determine temperatures in the CFRP during each strike.

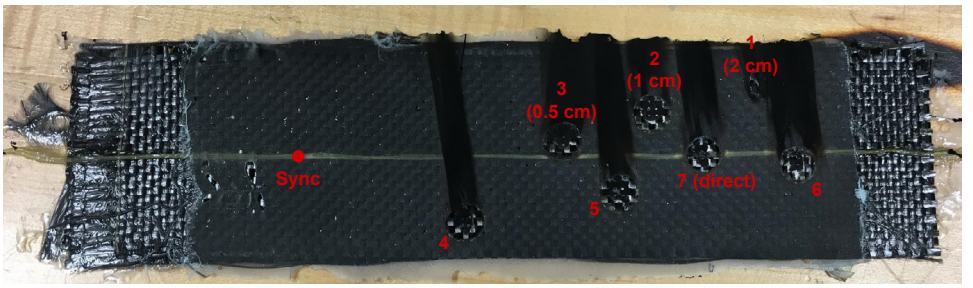

Fig. 16. Composite specimen with strike locations (as indicated in red).

7. HEL Strike Results—Localization

The HEL tests proved that a DOFS could be used to precisely locate the position of a laser strike on a composite material. After a single HEL strike, six peaks in temperature

were present, as would be expected for the configuration shown in Fig. 15 using the CFRP specimen in Fig. 6. Fig. 17 shows a schematic with the two beams directed at the composite. The left figure labels positions in the sensor at the sync beam or nearest the strike beam, and the right figure shows the temperature measurements during strike 6. Positions 1, 4,

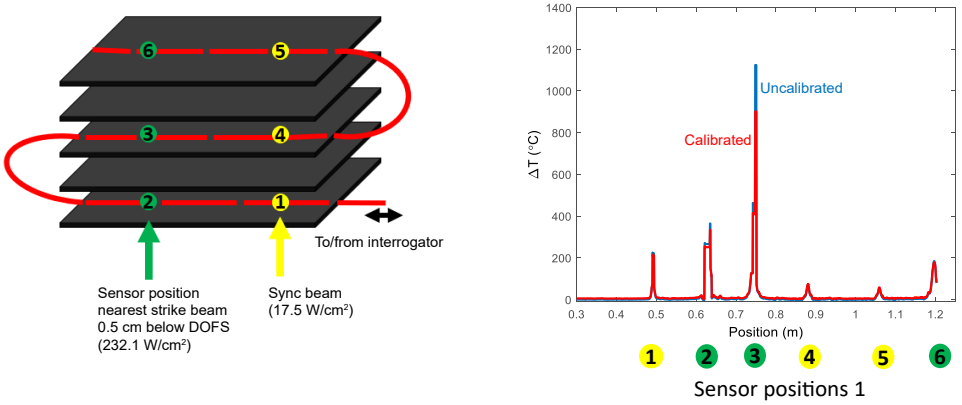

Fig. 17. HEL strike 6 and associated locations of strike on DOFS.

and 5 indicate locations of the sync beam through the different CFRP plies. Positions 2, 3, and 6 correspond to positions on the sensor nearest the strike beam through the depth of the composite. Positions 1 and 2 are on the front face of the composite where the laser is incident. Positions 3, 4, 5, and 6 measure temperatures from heat conducted through the composite as a result of the strike.

The right side of Fig. 17 is a snapshot of the temperatures in the composite during strike 6 approximately 1 s after the laser turned off. The peaks in the red curve correspond to actual temperatures the fiber sensor detected at each position. The blue curve shows an uncalibrated temperature change greater than 1100 °C at position 3. The red curve shows the importance of using the calibrated sensitivity, since the temperature shift at position 3 was actually closer to 900 °C. Note that position 3 (deeper in the specimen) is temporarily hotter than position 2 (on the front surface) just after the laser turns off because heat continued to conduct through the composite even after the laser strike ends. Each peak relates to an exact position on the fiber and is used to locate the HEL strike position for the strike beam. This demonstrates that the DOFS can reliably locate a HEL strike on a composite.

8. HEL Strike Results: Speed of Response

The DOFS speed of response varied depending on location of strike, conduction,convection, and other factors.[6] For example, Fig. 18 illustrates the delay between the sync beam and the strike beam during strike 3, when the HEL strike was 0.5 cm above the fiber. Fig. 18a shows the temperature readings at the six locations shown in Fig. 17 over a period of 60 s. In Fig. 18b, the initial temperature spike (red curve) at position 1 in the DOFS near 0.49 m is due to the sync beam (see Fig. 17), indicating a HEL turn-on time of t = 1.3002 s. The blue curve indicates a delay of roughly 420 ms before strike 3 is detected near position 0.56

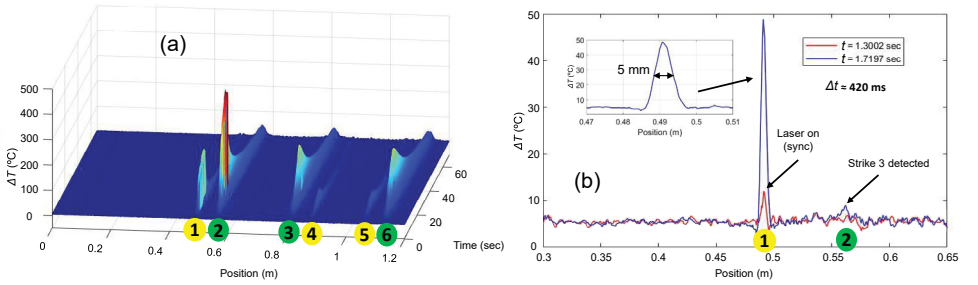

Fig. 18. HEL strike 3 (strike beam 0.5 cm above sensor). (a) Plot of temperature shift as a function of time and DOFS position. (b) Plot of temperature shift at two time samples, demonstrating delay between sync and strike beams.[6]

m (position 2 in Fig. 17) in the DOFS, 0.5 cm below the strike location (see Fig. 16), so that flames were directed upward away from the sensor.

The inset plot in Fig. 18b shows that the width of the thermal response of the sync beam is ~5 mm (full width at half the maximum shift). This is consistent with a $1/e^2$ HEL Gaussian beam width of 5.28 mm, as was measured before the composite tests using a Spiricon beam profiler with an optical wedge.

In contrast to strike 3, Fig. 19 shows the results near the beginning of strike 6. In this test, the strike beam was located 0.5 cm below the sensor, so flames were immediately directed upward toward the sensor. Both the strike and sync beams were observed to rise slightly in temperature at precisely the same time stamp. The resolution in time was limited by the data acquisition system that collects DOFS data at 23.8 Hz, with a sample taken every 40 ms, approximately. Hence the sensor detected the strike within approximately 40 ms or less.

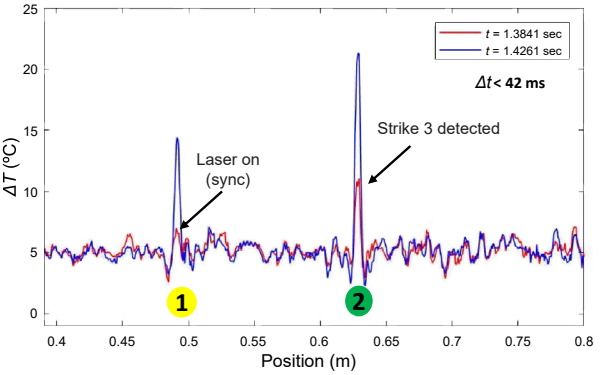

Fig. 19. HEL strike 6 (strike beam 0.5 cm below sensor)—no demonstrable delay between sync and strike beams.[6]

9. Conclusions

This work demonstrated the use of DOFS to rapidly detect and locate a directed energy strike on the surface of a composite. Before embedding fiber sensors into composite materials, and to accurately measure temperatures during a HEL strike, the fiber sensors needed to be properly calibrated to measure the correct temperature readings in the CFRP. The tube furnace was oriented horizontally to calibrate the DOFS. The high-temperature calibration was conducted up to 860 °C with less than 10% error. Above 860 °C, the cubic fit can be

used to extrapolate and predict sensor temperatures. The DOFS provides high-resolution sensing capable of precise location for the strike position while also identifying response speed of the sensors. Future work will be conducted to isolate strain from temperature during HEL strikes.

References

1. Freedberg, S. Jr., Army boosting laser weapons power tenfold, *Breaking Defense*, July 18 (2017).
2. Di Sante, R., Sensors, **15**(8), 18666 (2015).
3. Jenkins, B., Joyce, P., Mechtel, D., Milden, K., Elam, K., Watkins, J., Proc. SPIE, Smart Sensor Phenomena, Technology, Networks, and Systems Integration, 869308 (2013).
4. Rahim, N.A.A., Davis, M.A., Routhier, L., Chevalier, J., Bos, J., Kreger, S., Sanborn, E., Accuracy and survivability of distributed fiber optic temperature sensors, 53rd AIAA Aerospace Sciences Meeting, AIAA SciTech Forum (AIAA 2015-1920) (2015).
5. Garcia, J.D., Joyce, P.J., Brownell, C.J., J. Directed Energy, **6**(2) 119 (2017).
6. Jenkins, B., Joyce, P., Nelson, C., Kautzman, M., Proc. SPIE, Sensors and Smart Structures Technologies for Civil, Mechanical, and Aerospace Systems 2018, 105982D (2018).